# First-principles-based thermodynamic description of solid copper using the tight-binding approach

Sven P. Rudin,[1] M. D. Jones,[2] C. W. Greeff,[1] and R. C. Albers[1]

[1]*Los Alamos National Laboratory, Los Alamos, New Mexico 87545*

[2]*Department of Physics and Center for Computational Research, University at Buffalo, The State University of New York, Buffalo, New York 14260*

A tight-binding model is fit to first-principles calculations for copper that include structures distorted according to elastic constants and high-symmetry phonon modes. With the resulting model the first-principles-based phonon dispersion and the free energy are calculated in the quasi-harmonic approximation. The resulting thermal expansion, the temperature and volume dependence of the elastic constants, the Debye temperature, and the Grüneisen parameter are compared with available experimental data.

## I. INTRODUCTION

Density-functional theory (DFT) first-principles electronic-structure methods describe anomaly free solids such as elemental copper successfully. They achieve high accuracy for quantities such as bulk properties,[1] surface relaxation and lattice dynamics of the surface,[2] as well as the epitaxial Bain path and elastic constants.[3] DFT methods are routinely used to compute the zero-temperature internal energy $\Phi_0(V)$, but also can be used to calculate the free energy contributions from the ions $F_I(V,T)$ and the electrons $F_E(V,T)$ resulting in a complete equation of state

$$F(V,T) = \Phi_0(V) + F_I(V,T) + F_E(V,T). \tag{1}$$

However, the required computational effort is expensive, and an alternative efficient evaluation at all volumes and temperatures would be desirable.

In this paper we use the computationally less demanding tight-binding (TB) total energy model in conjunction with well chosen first-principles calculations. In particular, we use the functional fitting forms developed at the U.S. Naval Research Laboratory (NRL) for computing the total energy within the TB formalism, i.e., without an external potential.[4] The model is fit to and accurately reproduces a set of first-principles calculations with a speed-up of many orders of magnitude. In addition, transferability (i.e., a TB parametrization that is accurate for a wide variety of crystal structures and atomic arrangements) has been successfully demonstrated for semiconductors as well as for simple and transition metals.[4] We believe that the TB method can be used as a highly accurate, but computationally more efficient, surrogate for a full first-principles-based approach to calculate the equation of state for solids.

Copper is frequently used as a test material for theoretical methods.[5] In this paper we have (1) developed an improved fit for copper that is accurate for phonons and (2) used this model to calculate a wide range of temperature- and volume-dependent thermodynamic quantities.

Copper is furthermore widely employed as a pressure standard in high-pressure research.[6,7] This use is based on correcting $P(V)$ data taken along the shock Hugoniot[8] to room temperature. Such corrections employ model assump-

tions about the volume dependence of the Grüneisen parameter $\gamma(V)$, which is difficult to measure independently. Shock heating increases with pressure, making the corrections more significant at high pressure. It is therefore important to develop theoretical techniques for an accurate prediction of $\gamma$ for copper at high pressure.

Phonons play a major role in the calculations of thermodynamic quantities, and the TB fits are adjusted to more accurately calculate them. Structures corresponding to high-symmetry phonon modes are shown here to aid in refining the model; the resulting phonon density of states can then be used to determine the free energy and hence all thermodynamic quantities of interest. The precision required to calculate phonon frequencies is an order of magnitude higher than that for the lattice constant or bulk modulus,[9] making this a stringent test for the validity of the tight-binding approach in general and the copper model in particular.

The ion-ion free energy of Eq. (1) is often separated into harmonic and anharmonic parts

$$F_I(V,T) = F_H(V,T) + F_A(V,T). \tag{2}$$

Normally, the harmonic component is not a function of volume, but is calculated from the effect of small displacements about the zero-temperature equilibrium lattice. In our calculations, we use the quasiharmonic approximation, which considers small displacements at any fixed volume (lattice constant) within the harmonic approximation, and hence our phonon frequencies become volume dependent. However, our phonon frequencies are calculated at zero temperature for any given volume, and are not temperature dependent.

The anharmonic part of the free energy involves terms that arise from the potential energy of the lattice when it is expanded beyond the harmonic part to higher than second order. Such terms are needed at high temperatures, when the phonon amplitudes are large, and ultimately lead to melting. They are also needed to explain thermal expansion effects when the harmonic part is based on the equilibrium volume. The quasiharmonic approximation can handle thermal expansion and the Grüneisen parameter accurately through the volume dependence of the phonons at low temperature. At sufficiently high temperatures, the quasiharmonic approximation breaks down when the phonon amplitudes become

**65** 235114-1

large, and additional anharmonic phonon-phonon corrections are necessary [as indicated in Eq. (2)]. We have not included these anharmonic types of effects in our calculations. Hence we always set $F_A(V,T)=0$, and our calculations will become less reliable at very high temperatures (near melting).

In the following section we introduce the basic ideas of the tight-binding method and the first-principles method used to generate the fitting database, and then describe our TB fitting procedures. In the subsequent section we present calculated results for the thermodynamic properties and compare them with experiment.

## II. FITTING THE MODEL

### A. Tight-binding electronic structure

The tight-binding approach is essentially a parametrized version of the first-principles calculations and hence is orders of magnitude more computationally efficient. In DFT methods the secular equation

$$H\psi_{i,v}=\epsilon_{i,v}S\psi_{i,v},\qquad(3)$$

is constructed directly from approximate solutions to the full many-body Hamiltonian, and involves a self-consistent potential that is solved iteratively; whereas in the TB approach the elements of the Hamiltonian (and the overlap matrix) themselves have been parameterized. Only two-center terms are considered.[10] For the nonorthogonal tight-binding model described here this requires 73 fitted parameters.

Of those parameters, thirty each are used to describe the intersite matrix elements of the Hamiltonian and of the overlap matrix. For each combination of symmetries ($ll'm$) the form[11] is

$$h_{ll'm}(r)=(a_{ll'm}+b_{ll'm}r)e^{-c_{ll'm}^{2}r}f_c(r),\qquad(4)$$

$$s_{ll'm}(r)=(\bar{a}_{ll'm}+\bar{b}_{ll'm}r)e^{-\bar{c}_{ll'm}^{2}r}f_c(r),\qquad(5)$$

where $f_c=1/(1+e^{2(r-r_0)})$ is a multiplicative factor included to ensure a smooth cutoff with increasing distance. In our calculations we have set $r_0=16.0$ Bohr radii.

The remaining 13 parameters determine the on-site terms, which allows the parametrization to be applied to structures not included in the fitting database. A measure of the valence electron density

$$\rho=\sum_{i\neq j}e^{-\lambda^2 r_{ij}}f_c(r_{ij}),\qquad(6)$$

where $r_{ij}$ is the interatomic distance, serves to describe the on-site energy

$$e_\alpha=e_\alpha^0+e_\alpha^1\rho^{2/3}+e_\alpha^2\rho^{4/3}+e_\alpha^3\rho^2,\qquad(7)$$

for the three orbital types $\alpha$, i.e., $s$, $p$, and $d$. These terms are somewhat similar to an embedded-atom-like form in that the energy changes depending on the nearby arrangements of atoms, and may approximately account for self-consistency effects as the atoms move around.

TABLE I. Parameters used in the WIEN97 calculations. The choice for the $k$-point mesh size was not so much convergence as it was a balance between accuracy and a reasonable number of data points to fit.

| | |
|---|---|
| exchange-correlation functional | GGA (Ref. 13) |
| muffin-tin radius, $R_m$ | 2.0 a.u. |
| local orbitals (Ref. 14) | $s$, $p$, and $d$ |
| Gmax | 20.0 |
| R-MT*K-MAX | 9.0 |
| $k$-point mesh | $10^3$ (cubic, tetragonal) |
| | $6\times8\times12$ (frozen phonons) |
| | $6\times6\times10$ (trigonal) |
| Fermi-Dirac smearing | 0.002 Ry |

### B. Full potential LAPW method

The first-principles quality of the tight-binding model results from fitting to full potential linear augmented plane wave (LAPW) calculations using the reliable WIEN97 program suite.[12] The parameters for the first-principles calculations are listed in Table I.

The LAPW method divides space into spherical regions centered on the atoms and the remaining interstitial region. The radius of the spheres, the muffin-tin radius $R_m$, must be chosen such that the spheres do not overlap. The basis functions used to represent the wave function are adapted to the regions: radial solutions to the Schrödinger equation in the spheres, plane waves in the interstitial region. The wave functions then are found iteratively within density-functional theory, constrained to match at the boundaries of the different regions.

### C. Initial fitting procedure

We first fit the TB method to predict energy differences between the ground-state and nonequilibrium structures. The fitting database included first-principles energies calculated for the cubic structures. In addition to the total energies of these structures, it proved to be crucial to fit the energy bands at high-symmetry points in reciprocal space.[15,16] By decomposing the electronic wave function in terms of the symmetry character of the eigenvalues[17] the bands are guided to the correct ordering.

The total energies and the band energies can be calculated by starting with a very crude initial tight-binding model that ignores intersite terms;[15] the errors are then minimized utilizing standard nonlinear least squares algorithms.[18]

Figure 1 shows the $T=0$ fcc Cu phonon dispersion (see Sec. III A for details of the calculation) for the model from this initial fitting procedure.[15] The long-wavelength modes near $\Gamma$ are well described, the short-wavelength modes near the zone boundary display somewhat high frequencies, in particular the longitudinal modes.

The reasonable agreement for phonons near the zone center $\Gamma$ can be understood by considering the elements of the fitting database. The bulk modulus, i.e., a linear combination of the elastic constants, is implicitly included in the fit. While this does not guarantee accurate elastic constants, i.e., good
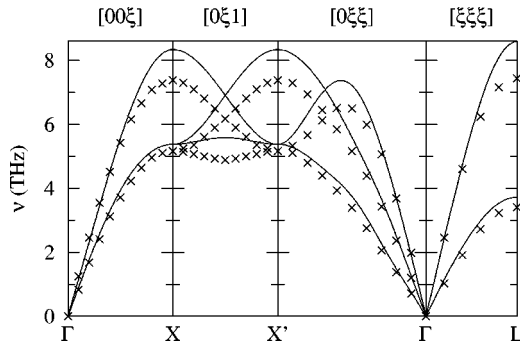
FIG. 1. Phonon dispersion of the initial tight-binding model for copper at the experimental equilibrium volume and zero temperature (solid lines). Crosses are measured neutron crystal spectrometer data at 80 K (Ref. 19).

agreement for the slopes of the dispersion near $\Gamma$, it does set the right scale. Furthermore, the fit includes the bcc structure, which is related to the fcc crystal by a tetragonal strain corresponding to the long-wave-vector limit of the longitudinal mode in the $[00\xi]$ direction. The database lacks any information related to the short-wave-vector modes.

### D. Fitting procedure with distorted structures

In order to construct a model with an improved phonon dispersion the database was expanded to include additional information on the phonons, in particular, structures that are snapshots of the crystal deformed by particular phonon modes, i.e., frozen phonons. The undistorted and distorted crystal structures are treated on the same footing in the first-principles calculations and the fitting procedure, implicitly including the differences in energy and hence the frequencies of the phonon modes.
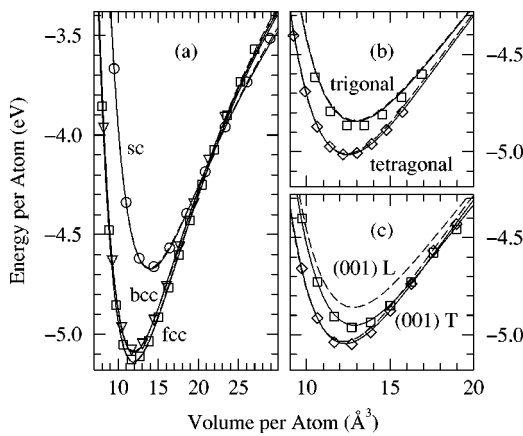


FIG. 2. Structures and volumes in the fitting database. Symbols are the WIEN97 results, dashed lines are the initial fit, solid lines are the improved fit for (a) simple structures (sc, bcc, fcc), (b) the fcc crystal with trigonal and tetragonal distortions, and (c) the fcc crystal with distortions corresponding to the longitudinal and transverse phonons at the reciprocal-space high-symmetry point $X$. The initial copper model is based on the data shown in (a), the improved model is fit to all the data.
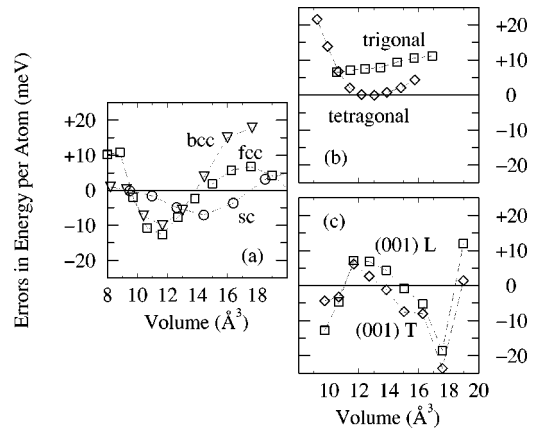


FIG. 3. Errors in the fitting for (a) simple structures (sc, bcc, fcc), (b) the fcc crystal with trigonal and tetragonal distortions, and (c) the fcc crystal with distortions corresponding to the longitudinal and transverse phonons at the reciprocal space high-symmetry point $X$. Dashed lines are to guide the eye.

The longitudinal and the transverse mode at the high-symmetry point X $[\mathbf{q}=(0,0,1)]$ were chosen because of the large discrepancy in frequency (see Fig. 1) and because the distorted structures require only a doubling of the unit cell. These distorted structures are considered as additional, distinct structures in the database, to be fit to over a range of volumes.

The initial fit for copper already contains some of the character of distortions related to the elastic constants: the bulk modulus is explicitly included in the energy as a function of volume, and the tetragonal distortion of the fcc crystal is somewhat reflected by fitting to the bcc structure. For completeness, tetragonally and trigonally distorted fcc crystals were added to the fit as distinct structures. These additional structures barely influence the model resulting from the fit; however, the fitting process converges much more quickly when they are included.

The cubic structures that were included in the initial fit differ from each other by an energy scale of fractions of
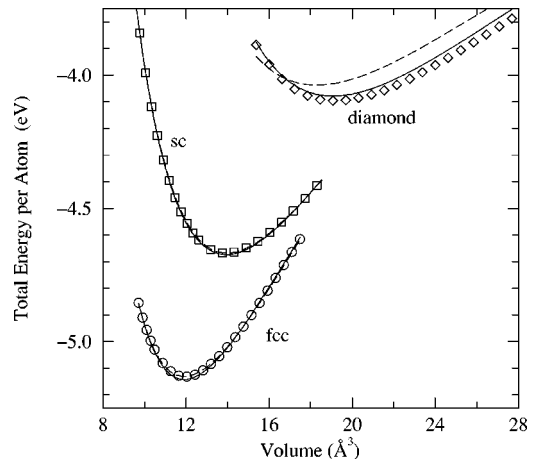


FIG. 4. Transferability of the improved model. Symbols are WIEN97 results, dashed lines are the initial tight-binding model, solid lines are improved tight-binding model.
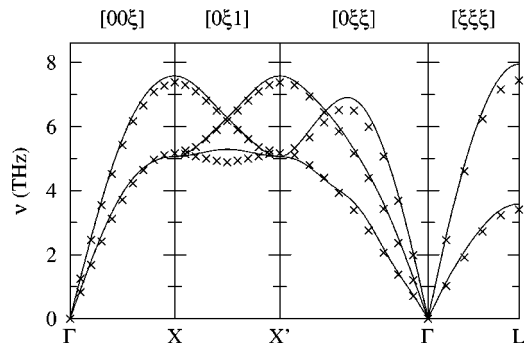
FIG. 5. Phonon dispersion of the improved tight-binding model (solid lines) compared to the experimental data (crosses) (Ref. 19). The slopes near $\Gamma$ and the two frequencies at $X$ are effectively part of the fitting data.
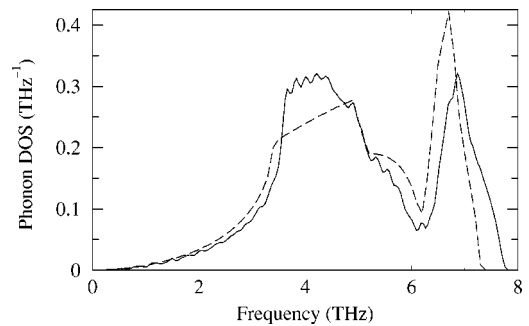


FIG. 6. Phonon density of states. The Dashed line is the eighth-nearest-neighbor model fit to the measured neutron crystal spectrometer data (Refs. 19,20), solid lines are calculated from the improved tight-binding model.

electron volts. Phonons require a model tuned to discern energies on a scale that is approximately an order of magnitude smaller. This could be a problem since the minimization procedure tends to ignore small energy differences. For frozen phonons at the zone boundary, where neighboring atoms move against each other, it turns out that amplitudes which are still within the harmonic regime can produce energies that differ from the undistorted structure by fractions of electron volts. The distortions corresponding to elastic constants, however, need to be exaggerated for them to give large enough energy differences. The trigonal distortion used here compresses the base angle from 90° to 75°, while the tetragonal distortion changes the $c/a$ ratio from unity to 1.9.

Figure 2 shows the energy values in the fitting database alongside those of the initial and improved tight-binding models. The volumes of the first-principles calculations are limited to structures where the muffin-tin radius $R_m$ is smaller than the nearest-neighbor distance, particularly for the strongly-distorted fcc structures the choice of $R_m$ $=2.0$ a.u. prohibits strong compression. No such limitations exist for the tight-binding approach; the volumes for which the model is appropriate will become clear in the next section.

Figure 3 shows the errors in the improved model's fit. Compared to the initial fit, errors for the simple, cubic structures remain about the same. The errors for the tetragonally distorted structures are small around the equilibrium volume (11.93 Å$^3$), but show a tendency to increase as the crystal is compressed. The form of the matrix elements [Eq. (4)] cannot be expected to allow a high-quality fit at all volumes; indeed when only a subset of data points are included in the fit the errors show no radical change.

Including the distorted structures in the fit improves the transferability of the model. Figure 4 shows the improved agreement between tight-binding and first-principles energies for the diamond structure, which is not included in the fit. The transferability to a structure of such a different coordination is not guaranteed, and our initial model did not reproduce the diamond energies well, nor did the model of the NRL group.[5]

Figure 5 shows the phonon dispersion calculated with the improved model. Including the distorted fcc structures

clearly refines the agreement with the measured values, though the curves do not overlap perfectly: the dispersion of the low-lying transverse modes in the $[0\xi1]$ direction shows a different character, and the high-frequency longitudinal modes remain somewhat large. The discrepancy of the longitudinal frequency at $L$ suggests including this data point in the fit. However, a first-principles, frozen-phonon calculation of this mode shows better agreement with the tight-binding model than with experiment and was therefore not added to the database.

Figure 6 shows the phonon density of states calculated with the improved model. The general shape agrees with the data calculated from the Born–von Kármán force constants fitted to the experimental phonon dispersion along high-symmetry directions.[19,20] The difference in maximum frequencies and the peak near 7 THz can be attributed to the discrepancy in the dispersion of the longitudinal mode near $L$ in the $[\xi\xi\xi]$ direction. The tight-binding density of states displays more structure around 4 THz, which may be due to modes in low-symmetry directions that are not part of the experimental force-constant model.

The distorted structures added to the fit indeed make for a model that is better suited for phonon calculations. However, while the additional constraints improve the total energies described by the model, the electronic band structure deteriorates. Figure 7 shows the electronic band structure along two sample high-symmetry directions of fcc copper at the experimental volume. While the initial model agrees well with the first-principles band structure, the model improved for thermodynamic quantities loses the good agreement. The resulting electronic density of states, shown in Fig. 8, shows the same discrepancy; however, the density of states at the Fermi energy is quite similar, which is important for the temperature-dependent influence of the electrons (see below). It is possible that a better or more flexible functional form for the distance dependence of the intersite Hamiltonian and overlap matrices are necessary to keep the good transferability and the good agreement with the individual energy bands.

## III. CALCULATIONS WITH THE TB MODEL

### A. Force constants

The force constants are calculated from the tight-binding model by the direct-force method,[21–24] which relies on evalu-
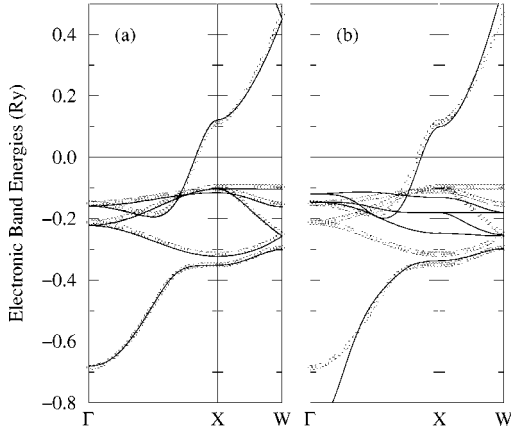
FIG. 7. Electronic band structure of fcc copper at the experimental volume. Circles are first-principles results, solid lines are the (a) initial and (b) improved tight-binding models.

ating the forces on all atoms in a simulation cell in which a reference atom $(\mathbf{0},i)$ has been displaced. The large simulation cell consists of primitive cells transposed by vectors $l$. Due to periodic boundary conditions on the simulation cell, the force on an atom $(l,j)$ is in response to the displaced reference atom $(\mathbf{0},i)$ as well as its images transposed by vectors $\mathbf{L}$

$$\mathbf{F}(l,j) = -\sum_{\mathbf{L}} \underline{\phi}(l,j;\mathbf{L},i)\cdot\mathbf{u}(\mathbf{0},i),\qquad(8)$$

i.e., we are actually calculating the cumulant force constant

$$\underline{\phi}^C(l,j;\mathbf{0},i) = \sum_{\mathbf{L}} \underline{\phi}(l,j;\mathbf{L},i).\qquad(9)$$

The components of the cumulant force constant are, in the harmonic regime, given by

$$\phi_{\alpha\beta}^C(l,j;\mathbf{0},i) = -\frac{\partial F_\beta(l,j)}{\partial u_\alpha(\mathbf{0},i)} \approx -\frac{F_\beta(l,j)}{u_\alpha(\mathbf{0},i)}.\qquad(10)$$

The calculation of the Hellmann-Feynman forces in the tight-binding approach is achieved by evaluating the analytic derivatives of the Hamiltonian and overlap matrix elements and of the onsite terms.
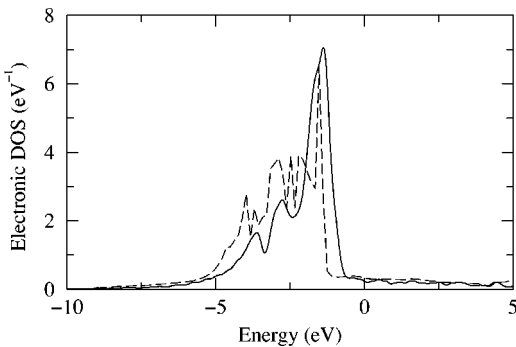


FIG. 8. Electronic density of states for fcc copper at the experimental volume. The Fermi energy is at $E=0$. Dashed line is the first-principles result, solid line is the improved TB model.

The frequencies of the phonons with a given wave vector $\mathbf{q}$ are found by diagonalizing the corresponding dynamical matrix $D(\mathbf{q})$, which in turn is the Fourier transform of the system's force constants

$$D_{\alpha\beta}(\mathbf{q}) = \frac{1}{M}\sum_{l,j,i} \phi_{\alpha\beta}^C(l,j;\mathbf{0},i)e^{i\mathbf{q}\cdot(\mathbf{r}_j-\mathbf{r}_i+l)}.\qquad(11)$$

If the force constants are known for every pair of atoms, the dynamical matrix and hence the frequencies are easily evaluated for any wave vector.

The direct-force method is exact within the quasiharmonic approximation and the particular model if the forces vanish inside the simulation cell. Computational resources often limit the system size such that the forces do not vanish at the boundary, as in the calculations presented here; the calculations are correct for wave vectors commensurate with the simulation cell and are a good approximation for intermediate values of $\mathbf{q}$.

The evaluation of Eq. (11) involves only the atoms in the simulation cell. In cases where the edge of the simulation cell limits the range of the forces before they actually vanish special care must be taken to ensure that no symmetries are lost. In particular, the inversion symmetry is lost if the reference atom $(\mathbf{0},i)$ is not in the center of the simulation cell. Atoms that break the inversion symmetry with respect to the reference atom have to be duplicated (with adjusted weight) and transposed with a basis vector of the simulation cell to reinstate the symmetry.

The cubic symmetry of the fcc crystal allows the calculation of the force constants at a particular volume with a single displacement of the basis atom. Distorted fcc structures no longer have the cubic symmetry, the calculation of the force constants therefore requires the forces to be evaluated for the basis atom displaced in all three Cartesian directions separately. For all calculations the simulation cell contained 108 atoms and a mesh of $4\times4\times4$ $k$ points was used.

### B. Thermodynamics

As indicated by Eq. (1), the free energy is the internal energy from the tight-binding calculation with entropic terms added from the electrons and the ions. In both terms the relevant physical quantity is the density of states (DOS). The electronic DOS, $n(E)$, the occupation of which is given by the Fermi distribution $f(E,T)=[e^{(E-E_f)/(k_BT)}+1]^{-1}$, determines the electrons' contribution to the entropy[25]

$$S_{el}(T) = -k_B\int [f\ln f + (1-f)\ln(1-f)]n(E)dE.\qquad(12)$$

The phonon DOS, $g(\omega)$, contributes through the zero-point energy,

$$U_{\text{zero}} = \frac{1}{2}\int_\Omega \hbar\omega g(\omega)d\omega,\qquad(13)$$

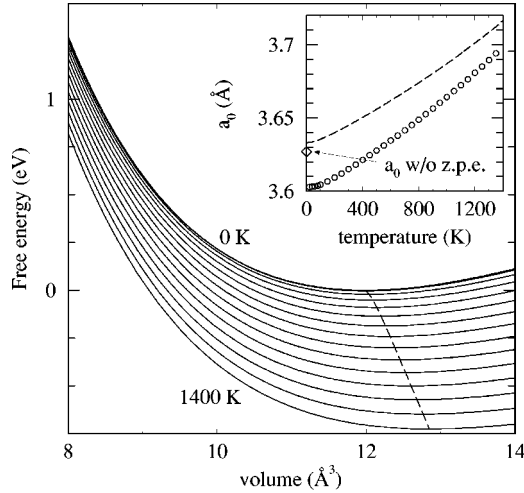as well as the temperature-dependent free energy[26]

FIG. 9. Free energy calculated in the quasi-harmonic approximation. The free energies are shown for temperatures from 0 to 1400 K in 100 K increments, relative to the $T = 0$ K free energy. Inset: calculated lattice constant (dashed line) and experimental values (circles) (Ref. 27) as a function of temperature. Also shown is the calculated lattice constant before taking into account the zero-point energy (diamond).

$$F_H(T,V) = k_B T \int_\Omega \ln[1 - e^{-\hbar\omega/k_B T}] g(V,\omega) d\omega. \quad (14)$$

Both DOS are calculated in the tight-binding calculations, the phonon DOS comes from evaluating the dynamical matrix for a fine mesh of wave vectors in the first Brillouin zone, and the electronic DOS results similarly from evaluating the eigenvalues on a fine mesh. A small Gaussian is used to smear the spectrum of the finite mesh (each phonon or electron energy eigenvalue at each $q$ or $k$ point in the Brillouin zone) to make it continuous. The width of the Gaussians is chosen as small as possible while keeping the DOS smooth and continuous. Both meshes are chosen fine enough so the resulting contributions to the free energy are converged. The contribution to the free energy from the electrons is on the order of a few percent of that of the phonons, although at low temperatures (where both contributions are very small) and small volumes the percentage rises to about 10%.

Figure 9 shows the resulting free energy as a function of volume for temperatures between 0 to 1400 K (at ambient pressure copper melts at 1356 K; melting is an anharmonic effect that lies outside the scope of the quasiharmonic treatment) in 100 K increments. A comparison with the free energy for the bcc phase shows the fcc structure at lower free energy for all temperatures and volumes, indicating that the model agrees with experiment in that respect.

The free energy as a function of volume and temperature determines the thermal expansion. The temperature-dependent lattice constant derived from the tight-binding model is shown in the inset of Fig. 9 along with the experimental values. As is typical for GGA calculations, the tight-binding model overestimates the equilibrium volume by 1.4%. The calculated linear expansion coefficient is com-
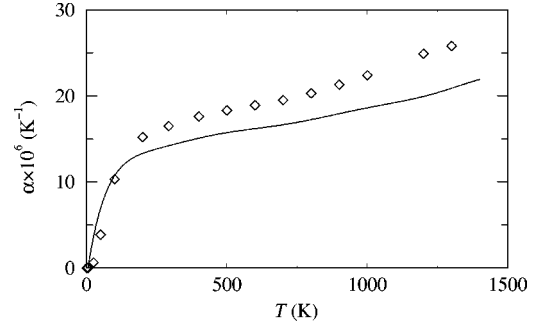


FIG. 10. Linear expansion coefficient for copper. Experimental values are represented as diamonds (Ref. 27), the result from the tight-binding model is the solid curve.

pared to experimental data in Fig. 10 and shows good agreement, in particular the characteristic temperature, which is determined by the phonon characteristic temperatures (see below).

The shape of the free energy as a function of volume and temperature directly provides the temperature dependence of the bulk modulus $B(T)$ which is calculated by fitting a second order Birch equation of state.[28] The bulk modulus is related to two of the elastic constants by $B(T) = \frac{1}{3}[C_{11}(T) + 2C_{12}(T)]$. The temperature dependence of the other elastic constants, determined by tetragonal $[C_{11}(T) - C_{12}(T)]$ and trigonal strain $[C_{44}(T)]$, is calculated in two steps. The $T = 0$ value results from calculating the energy of the appropriately strained crystal and finding the quadratic change. The temperature-dependent value is calculated by following the same procedure but with the free energy of the strained crystal, which is found by calculating the phonon DOS of that structure and then evaluating Eq. (14).

Figure 11 shows the calculated temperature-dependence of the elastic constants. The thermal expansion is implicitly included in the calculation of the bulk modulus, a derivative with respect to the volume. For the trigonal and tetragonal
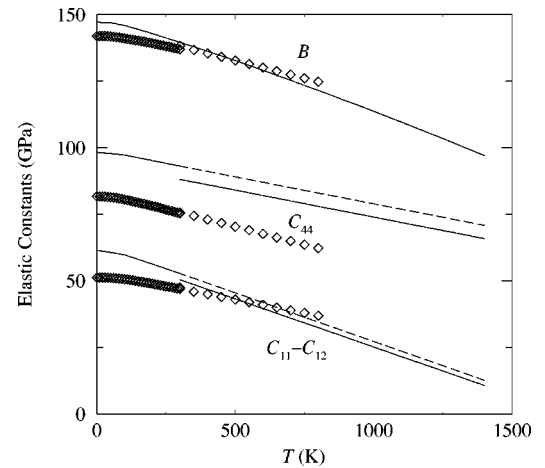


FIG. 11. Elastic constants as a function of temperature. Experimental values are represented as diamonds (Ref. 29). For the tetragonal and trigonal distortions we show the temperature dependence of the constant based on calculations at volumes appropriate for $T = 0$ and $T = 300$ K.
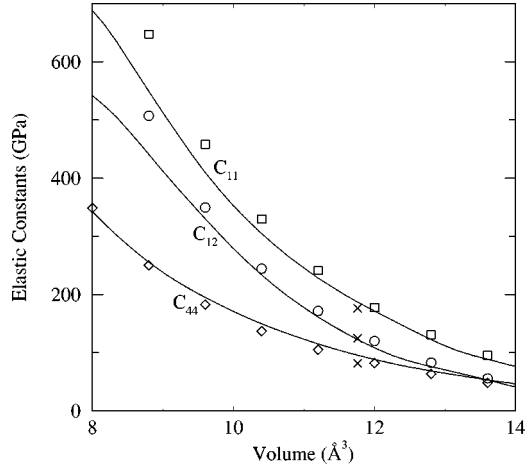
FIG. 12. Elastic constants as a function of volume. Experimental values at the equilibrium volume are shown as crosses (Ref. 29), first-principles results as symbols and results from the improved tight-binding model as solid lines.

strain the thermal expansion is accounted for by finding the equilibrium volume for each temperature and then calculating the effect of the strain on the free energy of that volume. Figure 12 shows the calculated $T=0$ elastic constants as a function of volume.

A similar calculation could be done to determined the temperature dependence of frozen phonons. However, it is important to point out that the calculated temperature dependence is done within a quasiharmonic approximation, and hence is valid only for not too high temperatures. What is more of interest is the temperature dependence due to anharmonic effects arising from large amplitudes of the atomic motions, which sample anharmonic parts of the interatomic potentials. These type of effects are probably best calculated in self-consistent phonon theories.[30–32] Such theories are a huge computational overhead beyond quasiharmonic theory, and are beyond the scope of this paper.

The phonon characteristic temperatures, which are defined as moments of the phonon density of states[33]

$$\ln(k_B \theta_0) = \langle \ln(\hbar \omega) \rangle_{\mathrm{BZ}}, \tag{15}$$

$$k_B \theta_1 = \frac{4}{3} \langle \hbar \omega \rangle_{\mathrm{BZ}}, \tag{16}$$

and

$$k_B \theta_2 = \left[ \frac{5}{3} \langle (\hbar \omega)^2 \rangle_{\mathrm{BZ}} \right]^{1/2}, \tag{17}$$

are shown in Fig. 13. The approximate rule of thumb $\theta_2 \approx \theta_1 \approx e^{1/3} \theta_0$ holds nicely for the calculated values (inset).

At temperatures below the phonon characteristic temperatures individual phonon modes must be considered separately, because they contribute to the crystal's thermal properties with weights depending on their frequency relative to the temperature. The weight of a mode of branch $s$ with wave vector $\mathbf{q}$ is determined by the heat capacity for that mode
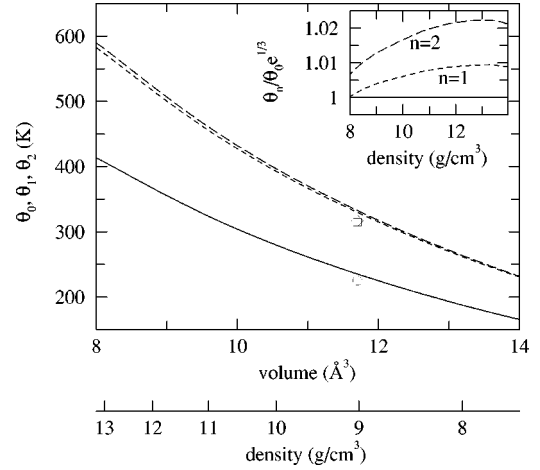


FIG. 13. Phonon characteristic temperatures. Symbols are from the experimental phonon density of states (Ref. 33), lines are the tight-binding results. Inset: deviations from the rule of thumb $\theta_2 \approx \theta_1 \approx e^{1/3} \theta_0$.

$$c_s(\mathbf{q}) = \frac{\partial}{\partial T} \frac{\hbar \omega_s(\mathbf{q})}{e^{\beta \hbar \omega_s(\mathbf{q})} - 1}. \tag{18}$$

The sum of these individual heat capacities as a function of temperature agrees well with calorimetric data; the comparison is plotted in Fig. 14 in terms of the Debye temperature $\theta_D$, which is found such that the Debye model's heat capacity

$$c_V = 9 k_B \left( \frac{T}{\theta_D} \right)^3 \int_0^{\theta_D / T} \frac{x^4 e^x}{(e^x - 1)^2} dx \tag{19}$$

is the same as the heat capacity calculated for the tight-binding model at the same temperature.

The shape of the Debye temperature plotted against temperature remains very similar with compression; the curve itself is shifted upwards with the same volume dependence as the characteristic phonon temperatures. The heat capacity of each individual phonon mode, combined with the Grüneisen parameter of that mode

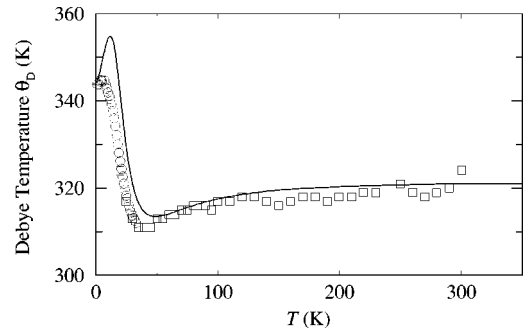$$\gamma_{\mathbf{q},s} = - \frac{d \ln \omega_s(\mathbf{q})}{d \ln V}, \tag{20}$$



FIG. 14. Debye temperature at the equilibrium volume. Symbols are from calorimetric experiments (Refs. 34,35), solid line is the tight-binding result.
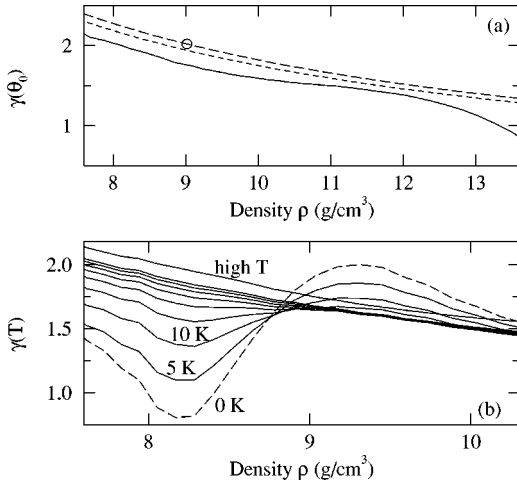
FIG. 15. (a) Grüneisen parameter calculated from $\theta_0$ (solid line), experimental value (circle), and $\gamma\rho$ = const (dashed lines). The long-dashed line goes through the data point of Wallace (Ref. 33), the short-dashed is from Hayes *et al.* (Ref. 36). (b) Calculated temperature dependence of the Grüneisen parameter. Shown are the results from $T = 0$ K to $T = 40$ K in 5 K increments as well as the high-temperature result.

determines the Grüneisen parameter

$$\gamma = \frac{\sum_{\mathbf{q},s} \gamma_{\mathbf{q},s} c_{v,s}(\mathbf{q})}{\sum_{\mathbf{q},s} c_{v,s}(\mathbf{q})}. \tag{21}$$

At high temperatures ($T > \theta_2$), where all phonon modes contribute equally, $\gamma \approx \gamma_0 = d \ln \theta_0 / d \ln \rho$. At low temperatures only the acoustic phonon modes contribute.

Figure 15 compares the tight-binding results for the Grüneisen parameter with available data. For densities up to near 13 g/cm$^3$ the results roughly agree with the rule of thumb that $\gamma\rho$ = const. Our values are slightly below the experimental values, indicating that the phonon frequencies do not increase with compression as rapidly as they should.

Figure 15 also shows the calculated temperature dependence of the Grüneisen parameter. At low temperatures ($T \lesssim 40$ K) the plot shows a fair amount of structure relative to the high-temperature curve. This can be understood from the phonon dispersion shown in Fig. 5, where the lowest branch is in the $[\xi\xi\xi]$ direction and becomes flat around 3 THz, frequencies that become relevant in their contribution to the specific heat at temperatures around a third of their energy, i.e., around 50 K. This branch is the lowest and hence appears first with increasing temperature, furthermore it appears with a lot of weight as there are eight spatial directions corresponding to these modes.

At low temperatures the phonon contribution to the heat capacity is proportional to $T^3$ and vanishes more rapidly than the electronic contribution, which is linear in temperature. Figure 16 shows the calculated coefficient of the electronic contribution to the heat capacity
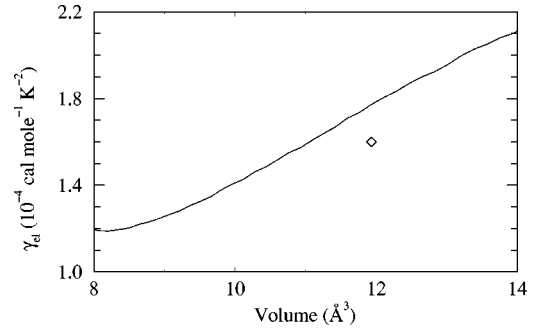


FIG. 16. Coefficient of the electronic contribution to the heat capacity. Diamond is the measured value (Ref. 37), solid line is the tight-binding calculation (using a $24^3$ $k$-point mesh with a Fermi-Dirac smearing of 225 meV).

$$\gamma_{\mathrm{el}} = \frac{\pi^2}{3} k_B^2 n(E_F), \tag{22}$$

which is proportional to the density of states at the Fermi energy $n(E_F)$. Compression of the crystal reduces $n(E_F)$, i.e., $\gamma_{\mathrm{el}}$ decreases monotonically.

## IV. SUMMARY

The work presented here is aimed at (1) improving the tight-binding fit of copper specifically for the calculation of thermodynamic properties and (2) investigating the transferability and range of applicability of the improved model. For the model to be reliable in calculating thermodynamic properties, it must produce a phonon dispersion in good agreement with experiment. The initial model was fit to first-principles calculations of the total energy at a series of different volumes for the cubic crystal structures. The database of first-principles calculations was extended here to include fcc structures distorted to reflect high-symmetry phonon modes and the elastic constants; fitting to the extended database yields the improved model which indeed delivers phonon frequencies significantly closer to the experimental values.

From the phonon density of states the free energy was calculated, in the quasiharmonic approximation, as a function of volume and temperature. The temperature dependence of the minimum of the free energy directly yields the thermal expansion and the linear expansion coefficient, both in good agreement with experiment. The elastic constants are somewhat improved over the initial model, though discrepancies with experiment remain evident.

The quantities in the previous paragraph depend on volumes only in the vicinity of the $T = 0$ equilibrium volume. The volumes used for the cubic and the distorted fcc structures in the fit extend over a wide range; the equilibrium volume is not treated any differently than other values (down to 9.7 Å$^3$, the smallest volume for which distorted structures were fit). This gives some confidence that the model applies to a range beyond the equilibrium volume and its immediate vicinity.

Within the quasiharmonic approximation the volume dependence of the phonon frequencies gives a nonzero Grün-

eisen parameter; the results calculated from the TB model roughly agrees with the empirical $\gamma\rho = $ const. The magnitude is somewhat low, i.e., the compression-induced stiffening of the crystal remains somewhat weaker than is experimentally measured.

The compression at which the model clearly fails can be seen from the Grüneisen parameter as well as the volume dependences of the elastic constants, the electronic contribution to the heat capacity, and the characteristic phonon temperatures. All of these entities vary monotonically with compression until the volume reaches approximately 8 Å$^3$, i.e., a density of roughly 13 g/cm$^3$, at which point unphysical behavior appears.

The unphysical behavior points to the limitations of the model. The Hamiltonian and overlap matrix elements are described by a functional form which can at best approximate the actual behavior within a limited range. For an extended range either the functional form must be modified, e.g., by including higher-order terms in Eq. (4), as has been done in a more recent NRL TB copper potential used in Ref. 5. The need for modification can also be seen in the electronic band structure, which is degraded by the fitting to distorted fcc structures.

[1] N. Troullier and J.L. Martins, Phys. Rev. B **43**, 1993 (1991).

[2] C.Y. Wei, S.P. Lewis, E.J. Mele, and A.M. Rappe, Phys. Rev. B **57**, 10 062 (1998).

[3] F. Jona and P.M. Marcus, Phys. Rev. B **63**, 094113 (2001).

[4] R.E. Cohen, M.J. Mehl, and D.A. Papaconstantopoulos, Phys. Rev. B **50**, 14 694 (1994); M.J. Mehl and D.A. Papaconstantopoulos, *ibid.* **54**, 4519 (1996); S.H. Yang, M.J. Mehl, and D.A. Papaconstantopoulos, *ibid.* **57**, R2013 (1998).

[5] Y. Mishin, M.J. Mehl, D.A. Papaconstantopoulos, A.F. Voter, and J.D. Kress, Phys. Rev. B **63**, 224106 (2001).

[6] W.J. Nellis, J.A. Moriarty, A.C. Mitchell, M. Ross, R.G. Dandrea, N.W. Ashcroft, N.C. Holmes, and G.R. Gathers, Phys. Rev. Lett. **60**, 1414 (1988).

[7] H.K. Mao, P.M. Bell, J.W. Shaner, and D.J. Steinberg, J. Appl. Phys. **49**, 3276 (1978).

[8] R. G. McQueen, S. P. Marsh, J. W. Taylor, J. N. Fritz, and W. J. Carter, in *High Velocity Impact Phenomena*, edited by R. Kinslow (Academic, New York, 1970).

[9] S. G. Louie, in *Electronic Structure, Dynamics, and Quantum Structured Properties of Condensed Matter*, edited by D. T. Devreese and P. van Camp (Plenum, New York, 1985), p. 335.

[10] J.C. Slater and G.F. Koster, Phys. Rev. **94**, 1498 (1954).

[11] The $(ll'm)$ symmetries are $(ss\sigma)$, $(sp\sigma)$, $(sd\sigma)$, $(pp\sigma)$, $(pd\sigma)$, $(dd\sigma)$, $(pp\pi)$, $(pd\pi)$, $(dd\pi)$, and $(dd\delta)$, as first suggested by J.C. Slater and G.F. Koster, Phys. Rev. **94**, 1498 (1954).

[12] P. Blaha, K. Schwarz, and J. Luitz, WIEN97, *A Full Potential Linearized Augmented Plane Wave Package for Calculating Crystal Properties* (Technical Universität Wien, Austria, 1999).

[13] J.P. Perdew, K. Burke, and M. Ernzerhof, Phys. Rev. Lett. **77**, 3865 (1996).

[14] D. J. Singh, *Planewaves, Pseudopotentials and the LAPW Method* (Kluwer, Boston, 1994).

[15] M. D. Jones and R. C. Albers (unpublished).

[16] D. A. Papaconstantopoulos, *Handbook of the Band Structure of Elemental Solids* (Plenum, New York, 1986).

[17] J. F. Cornwell, *Group Theory and Electronic Energy Bands in Solids* (North-Holland, Amsterdam, 1969).

[18] J. E. Dennis, Jr., D. M. Gay, and R. E. Welsch, ACM Trans. Math. Softw. **7**, 348 (1981).

[19] G. Nilsson and S. Rolandson, Phys. Rev. B **7**, 2393 (1973).

[20] P. H. Dederichs, H. Schober, and D. J. Sellmyer, *Landolt-Börnstein, Numerical Data and Functional Relationships in Science and Technology*, edited by K.-H. Hellwege and J. L. Olsen (Springer-Verlag, Berlin, 1981), Vol. 13a, p. 50.

[21] K. Kunc and R.M. Martin, Phys. Rev. Lett. **48**, 406 (1982).

[22] S. Wei and M.Y. Chou, Phys. Rev. Lett. **69**, 2799 (1992).

[23] W. Frank, C. Elsässer, and M. Fähnle, Phys. Rev. Lett. **74**, 1791 (1995).

[24] K. Parlinski, Z.Q. Li, and Y. Kawazoe, Phys. Rev. Lett. **78**, 4063 (1997).

[25] R. K. Pathria, *Statistical Mechanics* (Pergamon, Oxford, 1972), p. 139.

[26] R. K. Pathria, *Statistical Mechanics* (Pergamon, Oxford, 1972), p. 76.

[27] Y. S. Touloukian, R. K. Kirby, R. E. Taylor, and P. D. Desai, *Thermal Expansion: Metallic Elements and Alloys, Thermophysical Properties of Matter* (IFI/Plenum, New York, 1975), Vol. 12, p. 77.

[28] F. Birch, J. Geophys. Res. **83**, 1257 (1978).

[29] W.C. Overton, Jr. and J. Gaffney, Phys. Rev. **98**, 969 (1955); Y.A. Chang, L. Himmel, and J.P. Neumann, J. Appl. Phys. **37**, 3567 (1966).

[30] R.C. Albers and J.E. Gubernatis, Phys. Rev. B **23**, 2782 (1981).

[31] P. Choquard, *The Anharmonic Crystal* (Benjamin, New York, 1967).

[32] D. Wallace, *Thermodynamics of Crystals* (Dover Publications, Mineola, NY, 1998).

[33] Duane C. Wallace, Phys. Rev. E **56**, 1981 (1997).

[34] T.C. Cetas, C.R. Tilford, and C.A. Swenson, Phys. Rev. **174**, 835 (1968).

[35] D.L. Martin, Can. J. Phys. **38**, 17 (1960).

[36] D. Hayes, R. S. Hixson, and R. G. McQueen, in *Shock Compression of Condensed Matter*, edited by M. D. Furnish, L. C. Chhabildas, and R. S. Hixson (American Institute of Physics, Melville, 2000), p. 483.

[37] N. W. Ashcroft and N. D. Mermin, *Solid State Physics* (W. B. Saunders Company, Philadelphia, 1976), p. 49.